Supporting Information for Anderson et al.: Materials and Methods

Drillcores and Age Assignments

During the SHALDRIL II cruise, pre-Quaternary strata were recovered at four sites: Sites NBP0602A-3, 5, 6, and 12 (1) (Main Text Fig. 1). Eocene and Oligocene age assignments for Holes 3C (63°50.86'/ 54°39.21'; 340 m water depth) and 12A (63°16.35'/52°49.50'; 442 m water depth) are based on a combination of diatom, calcareous nannofossil, dinoflagellate cyst, and strontium isotope data (2, 3, 4), whereas the age interpretations for Holes 5C (63°15.11'/52°21.91'; 506 m water depth), 5D (63°15.09'/52°21.94'; 506 m water depth), 6C (63°20.03'/52°22.04'; 532 m water depth), and 6D (63°19.75/52°22.04'; 532 m water depth) rely solely on diatom biostratigraphy (2) (Table S1). A brief summary of the age assignments for each of the pre-Quaternary sections is given below. The placement of the assigned age intervals within the geomagnetic polarity timescale and key diatom biostratigraphic datums are shown in Fig. S1. These interpreted age ranges represent the narrowest/shortest intervals that can be constrained by biostratigraphy, not the total duration of deposition. Further discussion of the age assignments, along with diatom and calcareous nannofossil occurrence data and description of the strontium isotope results, is presented in Bohaty et al. (2). All ages are calibrated to the Gradstein et al. (5) timescale, and core nomenclature and terminology follow that described in the initial reports for the SHALDRIL project (1, 6).

Hole NBP0602A-3C

Hole 3C was drilled in the northern part of James Ross Basin in the Weddell Sea (63°50.86'S, 54°39.21'W), approximately 125 km to northeast of James Ross Island and Seymour Island (Main Text Fig. 1). This borehole is composed of a series of 8 cores drilled to a depth of ~20 meters below seafloor (mbsf) with an average recovery of ~35% (1). The core units are consecutively named Core 3C-1R_a at the top of the borehole to Core 3C-8R_a at the base.

Age assignments for Hole 3C are primarily based on diatom biostratigraphy, with supporting information provided by calcareous nannofossil and dinoflagellate cyst biostratigraphy and strontium isotope dating (2, 4). A very thin interval containing diatom assemblages of Late Pleistocene–Holocene age was recovered at the top of Hole 3C (3.00 to 3.15 mbsf). Paleogene strata were penetrated at shallow depths below this level, as indicated by the presence of characteristic Eocene diatoms, calcareous nannofossils, and dinoflagellate cysts in the lower portion of Core 3C-1Ra (3.55 mbsf). The biostratigraphic ranges of several diatom and dinoflagellate cyst taxa indicate a late Eocene age (~37 to 34.0 Ma) for the section (2) (Table S1; Fig. S1). One strontium isotope-based age estimate from Core 3C-5Ra (11.56 mbsf) provides support for this interpretation, indicating an age of 35.9±1.1 Ma. The sediments from this hole mostly consist of muddy to very fine sand that varies in color from greenish black in the upper portion of the hole (0–7.5 mbsf) to very dark greenish gray in the lower portion (7.5–~20 mbsf) of the core (1). It is assumed that the recovered Eocene section is relatively continuous, but a minor hiatus might be present at the lithological change ~7.5 mbsf (4).

Table S1, next page. Biostratigraphic datums used to constrain ages of pre-Quaternary strata. References 4 and 8-30 are cited in this table. Hj = Hajós (1976); GC = Gombos and Ciesielski (1983); P = Poore et al. (1983); W = Wise (1983); Hr = Harwood (1989); GB = Gersonde and Burckle (1990); BB = Baldauf and Barron (1991); HM = Harwood and Maruyama (1992); Berggren et al. (1995); Sc = Scherer et al. (2000); Wi = Wilson et al. (2000); HB = Harwood and Bohaty (2001); CG = Censarek and Gersonde (2002); W = Wilson et al. (2002); WI = Winter and Iwai (2002); ZG = Zielinski and Gersonde (2002); Bo = Bohaty et al. (2003); R = Roberts et al. (2003); WB = Whitehead and Bohaty (2003); B = Barron et al. (2004); WB = Williams et al. (2004); O = Olney et al. (2007); [a] *Gradstein et al. (2004);* [b] *Cody et al. (2008); average range model.*

Hole(s)	Fossil Group	Present/ Absent	Event	Taxon	Age (Ma)[a]	Age Calibration Source(s)	Compilation Age (Ma)[b]	Interpreted Age Constraint (Ma)
3C	diatom	present	LCO	*Pyxilla spp.*	~27–29	GC, BB, HM	-	≥~27–29
3C	diatom	absent	FO	*Cavitatus jouseanus* (early form)	~32	HB	-	≥~32
3C	diatom	present	LO	*Porotheca danica*	~32	GC, S	-	≥~32
3C	nannofossil	present	LO	*Transversopontis pulcheroides*	33.2	W	-	≥33.2
3C	diatom	present	LCO	*Hemiaulus caracteristicus*	33.2	GC	-	≥33.2
3C	diatom	absent	FCO	*Cestodiscus antarcticus*	33.4	H+	-	≥33.4
3C	dinoflagellate	present	LCO	*Deflandrea cygniformis*	33.7	WB, SH	-	≥33.7
3C	dinoflagellate	present	LCO	*Spinidinium macmurdoense*	33.7	WB, SH	-	≥33.7
3C	dinoflagellate	present	LCO	*Vozzhennikovia rotunda*	33.7	SH	-	≥33.7
3C	diatom	present	LCO	*Distephanosira architecturalis*	33.7	GC, H+	-	≥33.7
3C	diatom	absent	FO	*Stephanopyxis splendidus*	33.9	GC	-	≥33.9
3C	diatom	present	LO	*Pterotheca aculeifera*	34.0	GC	-	≥34.0
3C	diatom	absent	FO	*Rhizosolenia oligocaenica*	34.0	R	-	≥34.0
3C	diatom	present	FO	*Kisseleviella gaster*	~36	Hj, Hr	-	≤~36
3C	diatom	absent	LO	*Trinacria cornuta*	~37	S	-	≤~37
3C	diatom	present	FO	*Rocella praenitida*	~38.5	S	-	≤~38.5
3C	diatom	absent	LCO	*Triceratium inconspicuum* var. *trilobata*	~38.5	S	-	≤~38.5
3C	diatom	present	FO	*Hemiaulus caracteristicus*	~42	S	-	≤~42
5C-5D	diatom	absent	FO	*Fragilariopsis barronii*	4.16–4.36	BB, WI, WB	4.28–4.52	≥4.3
5C-5D	diatom	present	FO	*Thalassiosira complicata*	5.1–5.2	WI, WB	4.64–4.71	≤5.1
5C-5D	diatom	present	FO	*Thalassiosira inura*	4.9–5.6	CG, WI, WB	4.71–4.77	≤5.6
5D	diatom	present	LO	*Denticulopsis praedimorpha*	11.5–11.6	BB, HM	11.44	≥11.5
5D	diatom	present	LO	*Nitzschia denticuloides*	11.7–11.9	GB, BB, HM, CG, MB, Bo	11.72	≥11.7
5D	diatom	present	FO	*Denticulopsis ovata*	12.14	CG	9.64–12.14	12.1
5D	diatom	present	FO	*Denticulopsis dimorpha* var. *areolata*	12.2–12.8	BB, HM, CG	12.46–12.54	≤12.8
5D	diatom	present	FO	*Denticulopsis praedimorpha*	12.85–13.0	HM, CG	12.81-13.13	≤13.1
5D	diatom	present	FCO	*Nitzschia denticuloides*	13.6–13.7	GB, BB, HM, CG, MB	13.37–13.6	≤13.7
5D	diatom	present	FO	*Denticulopsis simonsenii*	14.20–14.30	GB, BB, HM, CG, MB	14.15–14.16	≤14.3
6C-6D	diatom	present	LO	*Thalassiosira complicata*	2.9–3.3	HM, ZG	3.36–3.44	≥2.9
6C-6D	diatom	present	LO	*Fragilariopsis aurica*	3.1–3.9	HM, ZG, WB	3.37–4.09	≥3.1
6C-6D	diatom	absent	FO	*Fragilariopsis interfrigidaria*	3.8–3.9	GB, HM, ZG, WI, WB	3.93–4.19	≥3.8
6C-6D	diatom	present	FO	*Fragilariopsis barronii*	4.16–4.36	BB, WI, WB	4.28–4.52	4.3
6C-6D	diatom	present	FO	*Thalassiosira complicata*	5.1–5.2	WI, WB	4.64–4.71	≤5.1
6C-6D	diatom	present	FO	*Thalassiosira inura*	4.9–5.6	CG, WI, WB	4.71–4.77	≤5.6
6C	diatom	present	FO	*Thalassiosira torokina* (early form)	8.6–9.1	BB, HM, WI	6.43–8.03	≤9.0
12A	diatom	present	LO	*Kisseleviella tricoronata*	~20.9	Sc, Wi, O	-	≥~20.9
12A	nannofossil	present	LO	*Dictyococcites bisecta*	22.8	P, Br, W	-	≥22.8
12A	diatom	present	LO	*Kisseleviella cicatricata*	23.3	Sc, W, O	-	≥23.3
12A	diatom	present	FO	*Cavitatus rectus*	28.4	B	-	≤28.4
12A	diatom	present	FO	*Cavitatus jouseanus* (sensu stricto)	31.1	R	-	≤31.1

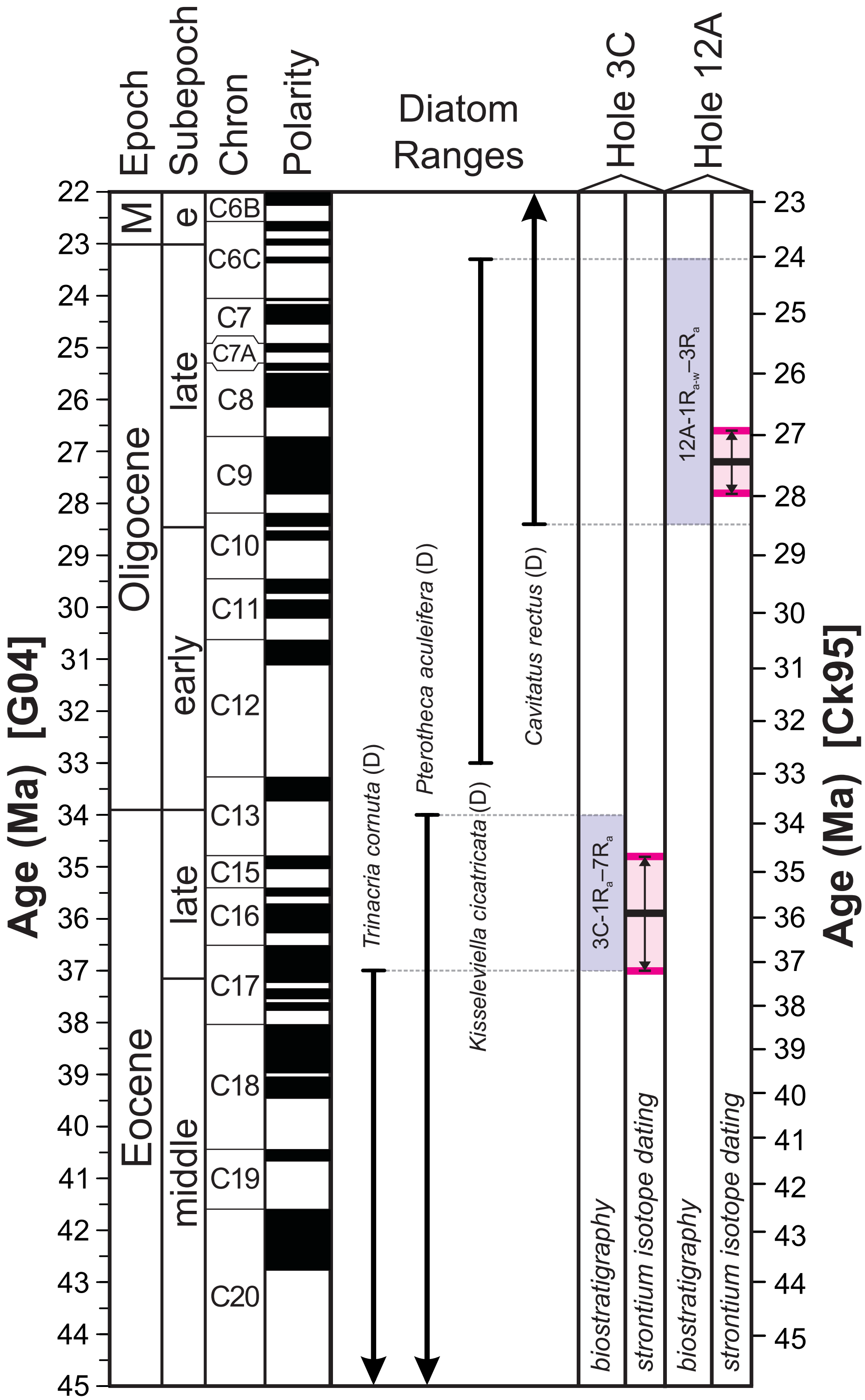

Age (Ma) [G04]
Age (Ma) [Ck95]
Epoch
Subepoch
Chron
Polarity
Diatom Ranges
Hole 3C
Hole 12A
M
e
Oligocene
late
early
Eocene
late
middle
C6B
C6C
C7
C7A
C8
C9
C10
C11
C12
C13
C15
C16
C17
C18
C19
C20
Trinacria cornuta (D)
Pterotheca aculeifera (D)
Kisseleviella cicatricata (D)
Cavitatus rectus (D)
3C-1Ra–7Ra
12A-1Ra-w–3Ra
biostratigraphy
strontium isotope dating
biostratigraphy
strontium isotope dating

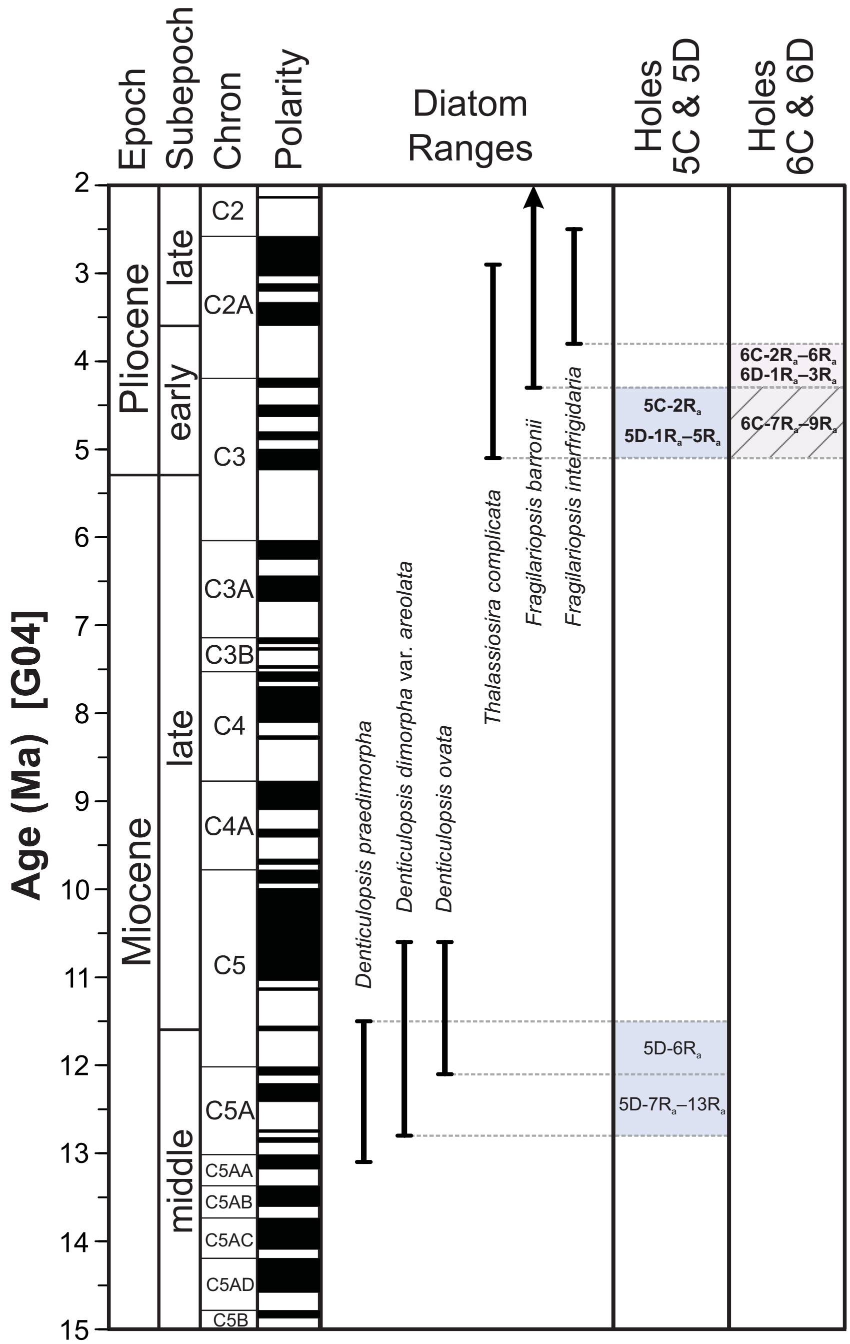

Figure S1, this and previous page. Key biostratigraphic datums and age assignments for drill cores.

Hole NBP0602A-12A

Hole 12A was drilled on the northeastern edge of Joinville Plateau, Weddell Sea (63°16.35'S, 52°49.50'W), approximately 115 km to the east of Joinville Island (Main Text Fig. 1). This borehole is composed of a series of 3 cores (Cores 12A-1R$_a$, -2R$_a$ and -3R$_a$) drilled to depth of 7.2 mbsf, with an average recovery of ~60% (1).

The thin, uppermost interval of Hole 12A (0.0–0.13 mbsf) contains a modern (extant) diatom assemblage, biostratigraphically constraining the age of the section to younger than 140 Ka (2). Below this level, between 0.15 mbsf to the bottom of the hole at 6.0 mbsf, the diatom assemblage contains several age-diagnostic taxa, including *Cavitatus jouseanus, C. rectus, Kisseleviella cicatricata,* and *K. tricoronata*. The combined ranges of these taxa provide an age estimate of 28.4 to 23.3 Ma for the lower section recovered in Hole 12A (Table S1; Fig. S1). The calcareous nannofossil assemblage is of limited diversity, but the presence of *Dictyococcites bisecta* supports an age assignment of late Oligocene or older (≥~22.8 Ma) for the section (2). A single strontium isotope age from a bivalve shell recovered in Core 12A-2R$_a$ (4.96 mbsf) also supports the biostratigraphic age interpretation, indicating an age of 27.2±0.6 Ma.

Holes NBP0602A-5C and 5D

Holes 5C and 5D were drilled on the northeastern edge of the Joinville Plateau, Weddell Sea (63°15.09'S, 52°21.94'W), approximately 135 km to the east of Joinville Island (Main Text Fig. 1). Overlapping intervals were drilled in the two holes. In Hole 5C, a highly-disturbed sample was recovered between 8.5 and 11.97 mbsf. Hole 5D was more successful, with a series of 13 cores (Cores 5D-1R$_a$ to 13R$_a$) to a depth of 31.4 m. The average core recovery in Hole 5D is ~40% (1).

Age assignments for Holes 5C and 5D are based solely on diatom biostratigraphy. The upper part of Core 5D-1Ra contains a Late Pleistocene–Holocene assemblage, which constrains the age of this unit to younger than 140 Ka (2). A hiatus is identified at the base of Core 5D-1Ra. The interval between Sample 5D-1Ra-1, 95 cm (8.95 mbsf) and Sample 5D-5Ra-1, 25 cm (16.25 mbsf) is assigned an early Pliocene age, with an interpreted age of 5.1 to 4.3 Ma (Table S1; Fig. S1). The poorly-consolidated, poorly-recovered core from Hole 5C (Core 5C-2R$_a$) is also included in this interval. Another hiatus is identified between Cores 5D-5R$_a$ and -6Ra (at ~18 mbsf), and Cores 5D-6R$_a$ through -13R$_a$ (18.80 to 30.36 mbsf) are assigned a middle Miocene age. The combined ranges of several diatom taxa constrain the age of the Miocene section recovered in Hole 5D to the interval between 12.8 and 11.7 Ma (2) (Table S1; Fig. S1). The presence of the diatom *Denticulopsis ovata* within Core 5D-6R$_a$ may allow further separation of the Miocene section into two subunits with different ages. The first occurrence datum of *D. ovata* is calibrated at 12.1 Ma; therefore, Core 5D-6R$_a$ (18.80 to 19.05 mbsf) is assigned an age between 12.1 and 11.7 Ma, and Cores 5D-7R$_a$ through -13R$_a$ (22.00 to 30.36 mbsf) are assigned an age between 12.8 and 12.1 Ma (2) (Table S1; Fig. S1).

Holes NBP0602A-6C and 6D

Holes 6C and 6D were drilled on the northeastern edge of the Joinville Plateau, Weddell Sea (63°20.27'S, 52°22.03'W), approximately 135 km to the east of Joinville Island and immediately south of Site 5 (Main Text Fig. 1). Overlapping sections were drilled in the two holes. Hole 6C penetrated to a depth of 20.5 mbsf with an average recovery of ~30%, and Hole 6D reached a depth of ~10 mbsf with an average recovery of ~45% (1). A series of 9 cores were drilled in Hole 6C (Cores 6C-1R_a to -9R_a), and 3 cores were drilled in Hole 6D (Cores 6D-1R_a to -3R_a).

The ages for Holes 6C and 6D are based on diatom biostratigraphy. Assemblages characteristic of the lower Pliocene are present in all cores recovered in these holes. Cores 6C-2Ra to -6Ra (~4.0 to 15.0 mbsf) and Cores 6D-1Ra to -3Ra (~5.0 to 10.0 mbsf) are assigned a well-constrained age of ~4.3 to 3.8 Ma (2) (Table S1; Fig. S1). In the lowermost section of Hole 6C (Cores 6C-8Ra and -9Ra, ~18.0 to 20.4 mbsf), low diatom abundance and poor preservation precludes precise biostratigraphic age control. The section recovered in Holes 6C and 6D, however, is interpreted to lie ~200 m stratigraphically above the lower Pliocene section recovered in Holes 5C and 5D (7). Therefore, age of the lowermost section of Hole 6C is constrained to an age younger than ~5.1 Ma (Fig. S1).

Sedimentology

Each of the drill cores was run through a GeoTek Multi Sensor Core Logger (MSCL) immediately after equilibration to room temperature following recovery from the sea floor and sectioning into 1 m lengths. MSCL data collection included magnetic susceptibility and *P*-wave velocity data. Gamma-ray density and electrical resistivity data were also collected, but did not contribute to interpretations. The magnetic susceptibility data were used as a proxy for the amount of terrigenous material compared to biogenic material in the cores. *P*-wave velocity was used in correlating the longer cores to seismic records.

Following the collection of the MSCL data, the cores were split and described on board ship. Visual lithology was described at sea including Munsell color code of the sediment color, smear slide description of the <250 μm fraction, and description of compositional, textural, and any other observed sedimentologic characteristics. Any lithologic boundaries were noted. A hand-held ER probe was then used as calibration of the MSCL ER measurements.

After the cruise, all sediment cores were transported in D-tubes to the Antarctic Research Facility at Florida State University where they are archived. Once there, the cores were x-rayed and the radiographs were used to produce counts of pebbles. X-rays were interpreted in Adobe Photoshop with the contrast adjusted for each image. Pebbles greater than 4 mm were counted and the reported value is the number counted per 5 cm of core.

Grain size analysis was conducted on a Malvern laser particle size analysis system at Rice University. Approximately 5 cc of sample was allowed to soak in de-ionized water with sodium hexametaphosphate as a dispersant to break up clasts and flocculated clay particles before samples were added to a magnetic stirrer. Sample was then added to the LPSA machine using a hand-held pipette. Duplicate measurements were made both of the same aliquot and of additional aliquots of the same sample to ensure consistency and lack of bias in sampling.

X-ray diffraction sample processing and analyses followed standard procedures (31). Bulk sediment samples were crushed, treated with 10% acetic acid and 5% H_2O_2 solution in order to remove carbonate and organic matter, respectively. The clay fraction (<2 µm) was separated in settling tubes. Approximately 40 mg of the clay fraction was dispersed and mixed with an internal standard consisting of a 0.4% MoS_2 suspension. The samples were mounted as texturally oriented aggregates on aluminium tiles and solvated with ethylene-glycol vapour at 60°C. The samples were then x-rayed (Rigaku Miniflex, CoKa radiation, 30 kV, 15 mA) in the range 3-40 °2θ with a scan speed of 0.02 °2θ/s. Additionally, the range 27.5–30.6 °2θ was measured with a step size of 0.01 °2θ in order to resolve more clearly the (002) kaolinite peak and the (004) chlorite peak.

Diffractograms were interpreted using the "MacDiff" software (32). The main clay mineral groups illite, chlorite, kaolinite and smectite are noted by their basal reflections at 10 and 5 Å (illite), 14.2, 7.1, 4.72 and 3.54 Å (chlorite), 7.1 and 3.58 Å (kaolinite), and ca 16.5 Å (smectite, after glycolation), after adjustment of the diffractograms using the MoS_2 peak at 6.15 Å. For semi-quantitative evaluations of the mineral assemblages, empirically estimated weighting factors were used on the integrated peak areas of the individual clay mineral reflections (33, 34, 35). The crystallinity of smectite and illite is expressed as the integral breadth (IB, D°2θ) of the 16.5 Å and 10 Å peaks, respectively. High values indicate poor crystallinities, whereas low values indicate good crystallinities. The composition of the illites can be estimated from the 5/10-Å peak area ratios (>0.4 for muscovite-like illites, <0.15 for biotite-like illites; 36) and the d-values of the (001) illite peak (<10.00 Å for muscovite, >10.10 Å for biotite).

Results of the lithologic and clay mineralogy analyses are given in Figure S2 and Table S2.

Grain Shape (Roughness)

We conducted Fourier Shape analysis on quartz grains from a representative set of samples from each drillcore. For this work, we used the 75–125 µm size fraction, and ~20 to 400 grains were analyzed from each sample. After chemical separation, the grains were photographed using a 10x objective on a petrographic microscope. Grain outlines were extracted from the grain images using a script run on ImageJ, a free image analysis software package. The grain outlines were used to calculate the Fourier Coefficients for

Core NBP0602A-6C

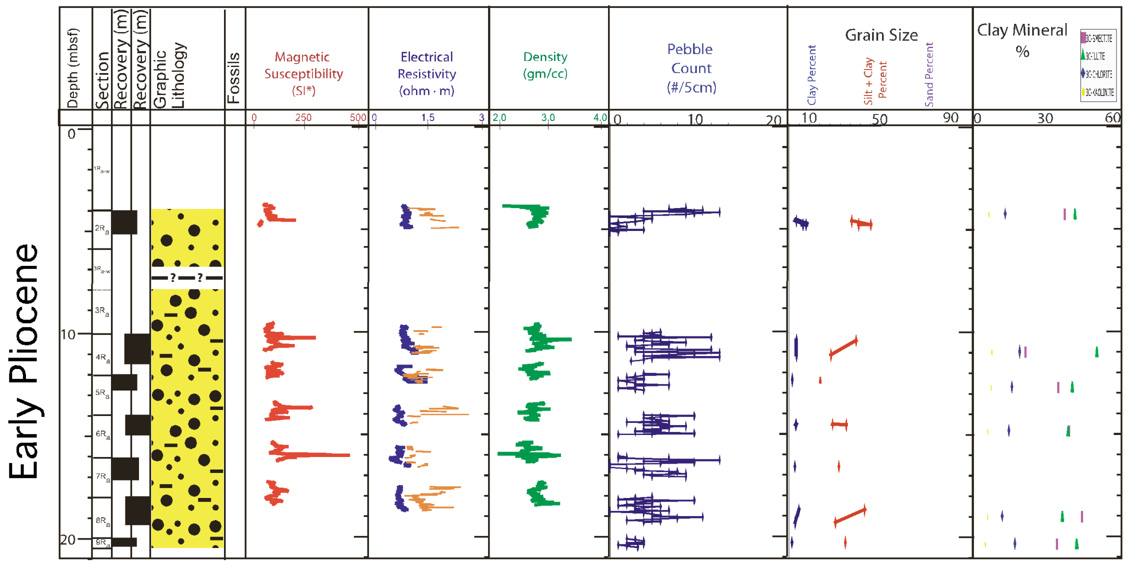

Core NBP0602A-5D

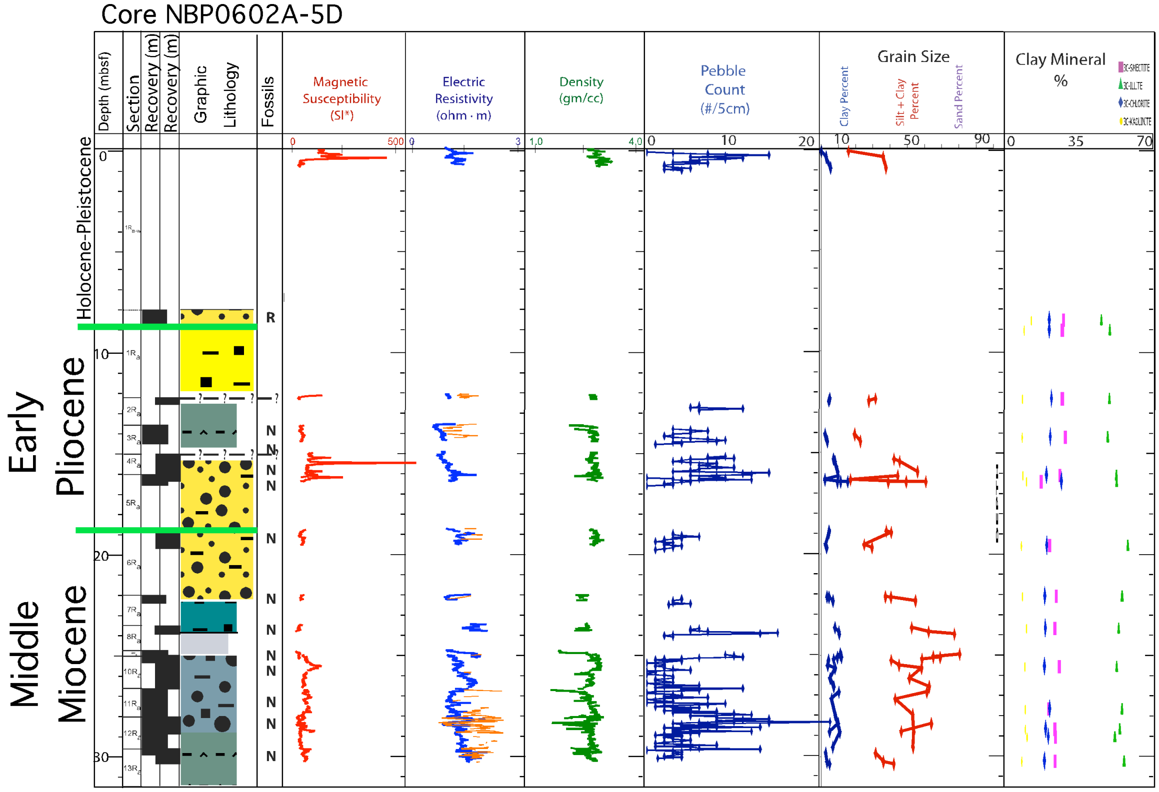

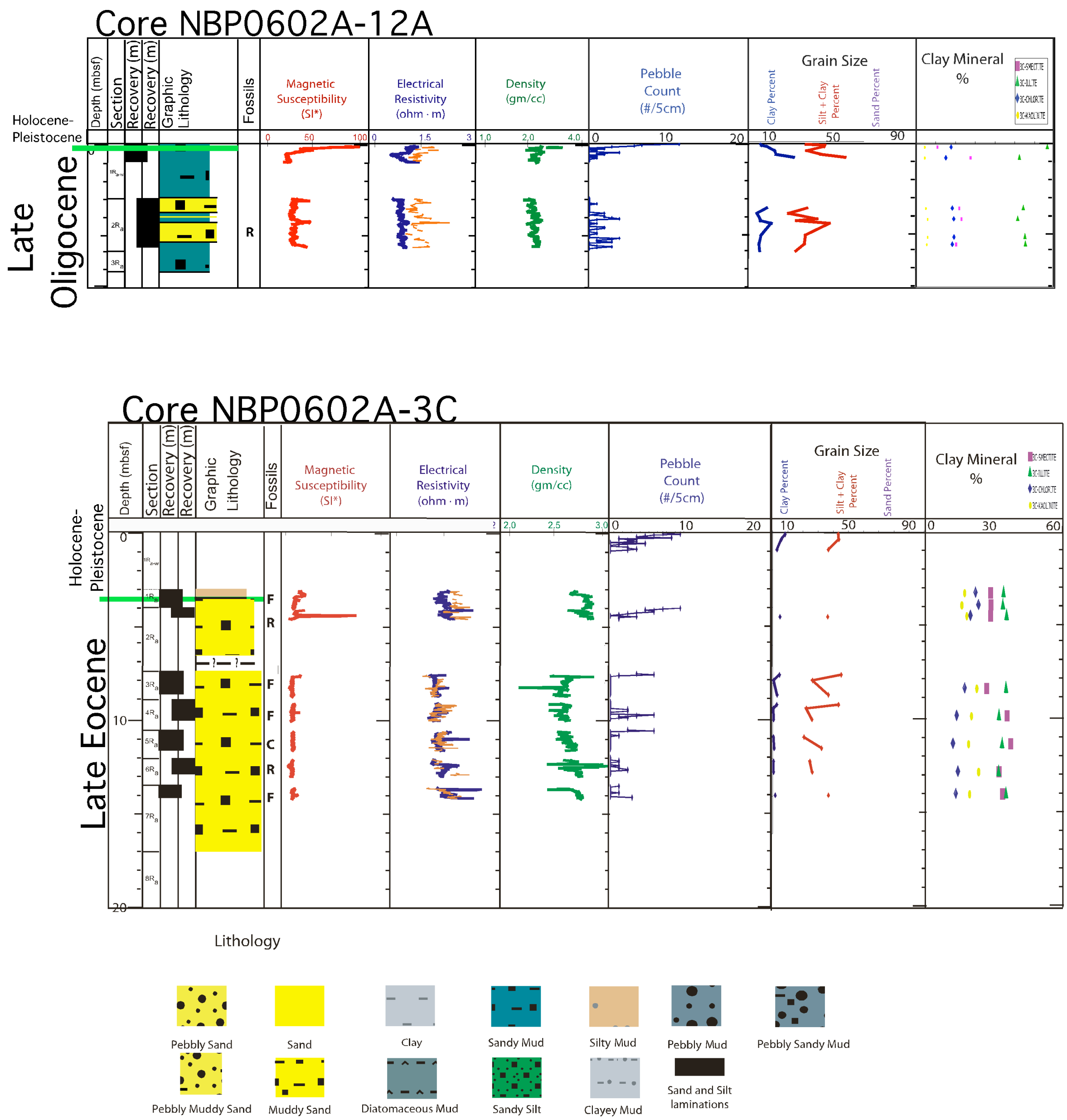

Figure S2, this and previous page. Lithologic logs for drill cores including multi-sensor core logger data.

Sample	% Smectite	% Illite	% Chlorite	% Kaolinite	Stratigraphy
3C-1, 16 cm	28.1	34.1	21.4	16.4	Quaternary
3C-1, 81 cm	28.3	33.8	22.8	15.1	Late Eocene
3C-2, 41 cm	28.1	35.5	19.1	17.3	Late Eocene
3C-3, 81 cm	26.4	35.2	16.5	21.9	Late Eocene
3C-4, 81 cm	35.7	32.1	12.8	19.4	Late Eocene
3C-5, 81 cm	37.1	33.4	11.3	18.2	Late Eocene
3C-6, 81 cm	32.0	31.9	13.4	22.7	Late Eocene
3C-7, 51 cm	33.6	35.3	12.5	18.6	Late Eocene
5D-1, 41 cm	26.1	44.4	19.1	10.4	Quaternary
5D-1, 91 cm	25.4	48.6	19.1	6.8	Early Pliocene
5D-2, 21 cm	25.4	48.4	20.2	6.0	Early Pliocene
5D-3, 71 cm	26.9	47.6	19.6	5.9	Early Pliocene
5D-4, 111 cm	24.2	51.7	17.8	6.2	Early Pliocene
5D-5, 41 cm	15.6	51.6	24.9	7.9	Early Pliocene
5D-6, 71 cm	19.4	57.2	17.8	5.5	Middle Miocene
5D-7, 11 cm	22.5	54.6	17.0	6.0	Middle Miocene
5D-8, 21 cm	22.2	52.7	17.2	8.0	Middle Miocene
5D-10, 61 cm	23.8	51.6	17.2	7.3	Middle Miocene
5D-11, 121 cm	18.8	54.5	19.3	7.4	Middle Miocene
5D-11, 261 cm	22.1	51.0	18.7	8.2	Middle Miocene
5D-12, 71 cm	21.8	53.4	17.4	7.4	Middle Miocene
5D-13, 61 cm	22.0	55.5	16.8	5.7	Middle Miocene
6C-2, 41 cm	38.0	42.4	13.3	6.3	Early Pliocene
6C-4, 101 cm	22.4	49.7	20.0	7.9	Early Pliocene
6C-5, 71 cm	35.4	41.3	16.0	7.3	Early Pliocene
6C-6, 81 cm	39.8	39.5	14.8	5.9	Early Pliocene
6C-8, 91 cm	45.3	36.8	12.0	5.9	Early Pliocene
6C-9, 21 cm	35.4	42.7	17.1	4.8	Early Pliocene
6D-2, 71 cm	34.7	44.9	14.7	5.7	Early Pliocene
6D-3, 61 cm	41.2	36.0	15.0	7.8	Early Pliocene
12A-1, 21 cm	10.9	66.7	17.9	4.5	Quaternary
12A-1, 81 cm	27.3	53.1	15.1	4.5	Late Oligocene
12A-2, 61 cm	22.0	54.4	18.5	5.0	Late Oligocene
12A-2, 121 cm	23.1	51.6	19.3	6.0	Late Oligocene
12A-2, 221 cm	20.7	54.0	19.3	5.9	Late Oligocene
12A-2, 261 cm	21.0	55.1	18.4	5.5	Late Oligocene

Table S2. Clay mineralogical data.

harmonics 1-20 using a Fortran code based on the equations of Ehrlrich and Weinberg (37).

In the interpretation of differences in grain shape, it is important to keep in mind that the grain shape is also influenced by sediment provenance (38) and sediment transport distance (39). Given the depth of the cores and distance from land, plus the unsorted nature of the sediments, we assume that sand size material is transported to the sites by icebergs. Therefore, the changes in grain shape most likely truly reflect changes in degree of glaciation.

Although direct comparisons between data collected from different regions and from different sediment size fractions are problematic (40, 41), a comparison with similar studies does allow the placement our roughness coefficient results into a paleoenvironmental context. Dowesdwell et al. (42) sampled a transect of environments from glacial to glacial marine environments from Baffin Island, Canada. They found that that the 150–500 micron grains imaged via SEM analysis from glacial deposits had higher roughness coefficients than the same sized grains from marine sediments. Again, caution should be made in trying to compare values; Dowesdwell et al. (42) found glacial deposits to have roughness coefficients from harmonics 16-20 of 0.0055-0.0069 and glacial marine deposits to have roughness coefficients of 0.004-0.0049. These values have similar trends as observed in our dataset.

Grain shape results are presented in Table S3.

Grain Surface Texture

We examined in detail a total of ten sand grains per sample from 18 stratigraphic intervals for surface morphological characterization. Samples were acquired from drill core and piston cores as part of the SHALDRIL program as described above. Additional samples from Seymour Island were generously provided by the United States Polar Rock Repository (D6-03, D6-05, D6-07).

In all sample preparation steps, we took great care to preserve sample morphology and avoid generating any surface features (43). We sieved samples at 63 μm and then made splits to reduce sample size with representative grain populations. All quartz grains in the final split were identified and mounted for analysis. Specimens were then coated with approximately 20 nm of a conductive material. Grains were examined using a FEI Quanta 400 high-resolution field emission scanning electron microscope in high vacuum mode. We verified the composition of each grain as pure SiO_2 with Energy Dispersive X-Ray Spectroscopy.

Textural features of the quartz grains were identified based on the criteria and examples from Mahaney (44). Fifteen individual microtextural features were recorded as not-present, low abundance, medium abundance, or high abundance for each individual

Sample	Avg. Rc 16-20	Standard Dev (16-20)
3C-1_13-14G75toG125	0.0075988	0.0002173
3C-1_39-40G75toG125	0.0072547	0.0001831
3C-3_8-9G75toG125	0.0074375	0.0001969
3C-3_114-115G75toG125	0.0072845	0.0001617
3C-7_47-48G75toG125	0.0080149	0.0002321
5D-1_10-11G75toG125	0.0070456	0.0001583
5D-2_26-27G75toG125	0.0047141	0.0001557
5D-3_47-48G75toG125	0.0055821	0.000275
5D-4_27-28G75toG125	0.0056587	0.0002542
5D-5_27-28G75toG125	0.0055764	0.0001377
5D-6_1-2G75toG125	0.0061939	0.0001414
5D-6_83-84G75toG125	0.0063487	0.0001322
5D-7_4-5G75toG125	0.0064512	0.0002202
5D-10_44-45G75toG125	0.00632	0.0001268
5D-11_5-6G75toG125	0.0065903	0.0002144
5D-13_70-71G75toG125	0.0065686	0.000147
6C-2_61-62G75toG125	0.005542	0.000264
6C-6_46-47G75toG125	0.0063338	0.0001931
6C-8_122-123G75toG125	0.0059574	0.0003224
6D-1_13-14G75toG125	0.0058608	0.000308
6D-2_0-1G75toG125	0.0052674	0.0005116
6D-3_122-123G75toG125	0.0059807	0.0002431
7A-1_2G75toG125	0.0066092	0.0002229
12A-1_4-5G75toG125	0.0060853	0.0002705
12A-1_37-38G75toG125	0.0059199	0.0001466
12A-2_67-68GG75toG125	0.0059388	0.0001618
12A-2_225-226G75toG125	0.0059014	0.0002115

Table S3. Mean roughness coefficient of quartz sand grains for Fourier shape harmonics 16-20 (37). Harmonics 16-20 are thought to describe the angularity of the grain rather than its form and thus are best at reflecting depositional processes (40, 42). Outside of the Eocene section, in general, rougher grains represent a greater importance of glacial processes. See supplementary information text for a more detailed discussion on grain roughness.

grain for ten grains per sample. The grain surface texture column shown in figure 3 (main text) is an average occurrence of glacially derived microtextures plotted on a scale of zero abundance, low abundance (<33%), medium abundance (33%-67%) and high abundance (67%-100%).

We focused on the glacially-formed microtexture category as established by Sweet and Soreghan (45). The glacially derived, sustained high stress features consist of crescentic gouges, straight grooves, curved grooves, and deep troughs. Examples of some of the most diagnostic features are illustrated in Figure S3. The average occurrence of glacially derived microtextures was established by calculating the mean of the four glacially-derived microtextures over each stratigraphic interval.

Palynology

Seventy-two samples were collected to conduct detailed palynological analysis of the SHALDRIL cores. Twenty samples were collected from Hole 3C, twelve samples were collected from Hole 12A, twenty-two samples were collected from Hole 5D, and sixteen samples were collected from Holes 6C and 6D.

All samples from this study were processed via a standard palynological technique suited for Antarctic sediments. For each sample, about 10 g of dried sediment was weighed to allow calculation of palynomorph concentration per gram of dried sediment. The sediment was also spiked with a known quantity of *Lycopodium* spores to allow computation of the absolute abundance of palynomorphs in the sample. Acid soluble minerals present in the sediment were digested in HCl and HF acid to remove carbonates and silicates. The palynomorphs were then concentrated by filtration through a 10-µm mesh sieve. The entire residue obtained was mounted on microscopic slides for analysis. Analysis was conducted under 60· oil immersion objective with a BX41 Olympus microscope. For samples with sufficient palynomorph abundance, a minimum of 300 palynomorphs were tabulated per sample. For samples with low abundance, the entire residue was tabulated. A database of all palynomorphs recovered was prepared and key species were photographically documented using QCapture software.

The palynological results are presented in Table S4. Additional details of the palynological studies are reported in Warny and Askin (2, 3).

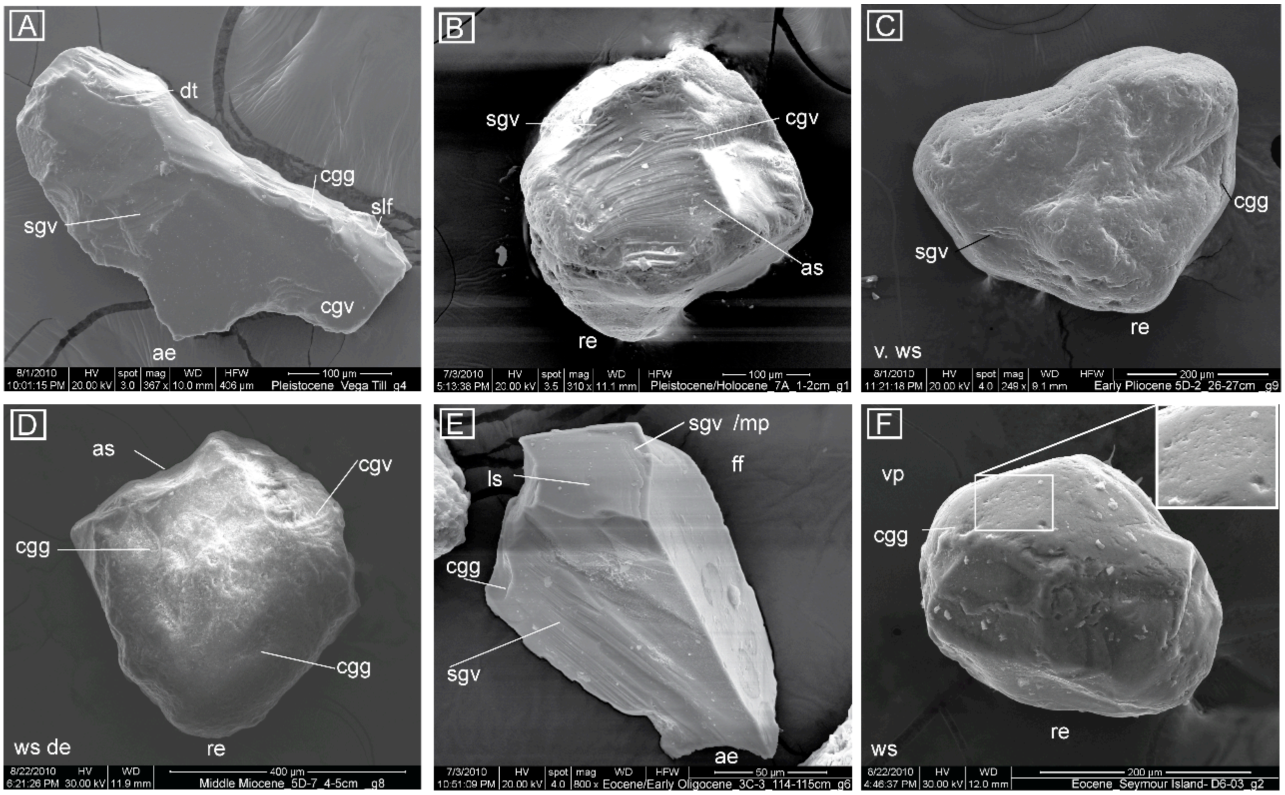

Figure S3. Scanning Electron Microscope (SEM) images of sand grains from samples taken at different intervals within the sampled section and illustrating glacial versus non-glacial surface features. **A)** Grain from Pleistocene till illustrating sustained high-stress microtextures indicative of glacial erosion and transport, including curved grooves (cgv), straight grooves (sgv), crescentic gouges (cgg), subparallel linear fractures (slf) and deep troughs (dt). **B)** Grain from Pleistocene till with rounded edges (re), abundant curved grooves (cgv), straight grooves (sgv) and arc shaped steps (as). **C)** Sub-rounded, highly weathered grain from the early Pliocene section, with rounded edges (re), straight grooves (sgv) and cressentic gouges (cgg). **D)** Grain from middle Miocene section with weathered surface (ws), faint dissolution etching (de) and rounded edges (re) superimposed on older cresentic gouges (cgg), curved grooves (cgv) and arc shaped steps (as). **E)** Fresh and angular grain from the late Eocene with angular edges (ae) and little/no surface weathering. There are numerous fracture faces (ff), linear steps (ls), crescentic gouges (cgg), straight grooves (sgv) and mechanically upturned plates (mp). **F)** Rounded grain from the Eocene La Meseta Formation, Seymour Island, Antarctica. The grain has rounded edges (re) and a weathered surface (ws) and features include crescentic gouges (cgg) and v-shaped impact pits (vp).

Table S4, next page. Detailed results from pollen and spore work.

CORE	BOTTOM DEPTH	*Nothofagidites* sp.*fusca* gp.	*Nothofagidites brassii* gp.	*Nothofagidites menziesii* gp.	Conifer pollen	Proteaceae	Other angiosperm pollen	Cryptogam spores
PLIOCENE								
6C-2	58	0	0	0	0	0	0	0
6C-2	114	0	0	0	0	0	0	0
6D-1	11	0	0	0	0	0	0	0
6D-2	10	0	0	0	0	0	0	0
6D-2	49	0	0	0	0	0	0	0
6D-2	92	0	0	0	0	0	0	0
6D-3	5	0	0	0	0	0	0	0
6D-3	40	0	0	0	0	0	0	0
6D-3	73	0	0	0	0	0	0	0
6D-3	127	0	0	0	0	0	0	0
6C-4	39	0	0	0	0	0	2	0
6C-4	131	0	0	0	0	0	0	0
6C-5	25	0	0	0	0	0	0	0
6C-6	70	0	0	0	0	0	0	0
6C-7	96	0	0	0	0	0	0	0
6C-8	56	0	0	0	0	0	0	0
6C-8	124	0	0	0	0	0	0	0
6C-9	32	0	0	0	0	0	0	0
5D-1	42	0	0	0	0	0	0	0
5D-2	18	0	0	0	0	0	0	0
5D-3	45	0	0	0	0	0	0	0
5D-4	13	0	0	0	0	0	0	0
5D-4	65	0	0	0	0	0	0	0
5D-4	123	0	0	0	0	0	0	0
5D-5	24	0	0	0	0	0	0	0
5D-6	12	0	0	0	0	0	0	0
5D-6	65	0	0	0	0	0	0	0
MIOCENE								
5D-7	29	7	0	0	1	0	1	1
	39	9	1	0	5	1	1	1
5D-9	45	13	0	0	3	1	0	0
5D-10	14	5	0	0	1	0	1	0
	88	11	0	0	3	2	0	0
	173	6	0	0	2	0	1	1
5D-11	66	10	0	0	2	1	1	1
	153	4	0	0	3	1	1	1
	232	12	0	0	4	1	4	0
	315	16	0	0	8	1	3	1
5D-12	11	4	1	0	1	0	1	1
	85	12	1	1	6	0	4	3
5D-13	65	8	1	0	9	1	1	2
OLIGOCENE								
12A-1	32	10	0	0	3	1	2	1
	64	13	0	0	8	1	3	1
	97	25	0	1	12	1	3	3
12A-2	35	21	0	0	19	1	5	3
	71	30	1	0	13	2	8	3
	105	24	0	1	16	1	7	2
	146	28	2	0	17	1	6	2
	173	20	1	1	26	1	6	2
	204	32	2	1	19	4	5	2
	234	20	1	0	29	2	8	4
	264	17	1	0	12	1	4	3
EOCENE								
3C-1	56	47	1	0	7	0	6	3
	90	64	2	1	14	1	7	4
3C-2	12	59	0	0	9	2	5	4
	31	44	0	0	20	1	3	5
3C-3	13	75	0	1	14	1	4	2
	61	69	0	0	15	0	5	5
	97	76	1	1	12	1	5	1
3C-4	12	69	1	1	18	1	4	2
	51	69	3	0	15	4	1	6
	87	65	3	0	17	2	2	4
3C-5	12	72	2	0	15	1	2	3
	56	70	0	1	19	0	4	1
	85	70	2	1	16	2	2	4
3C-6	12	64	2	1	20	2	4	3
	51	76	3	1	12	1	1	4
	85	79	0	0	14	1	3	1
3C-7	8	72	3	2	16	1	2	3
	31	73	1	1	15	1	7	1
	59	74	5	3	12	1	2	2

Tectonics

A review of regional tectonics is provided here for context of the glacial and biologic changes documented in this study. Figure S4 shows a seismic line collected for drill core location. Table S5 lists tectonic events by age.

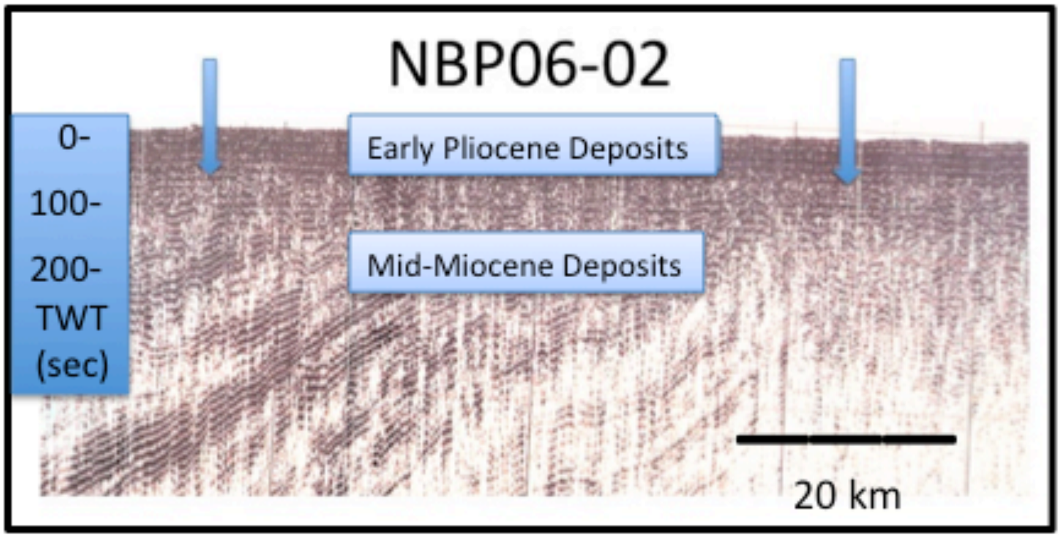

Figure S4. Seismic profile NPB06-10 across the South Orkney Plateau showing prominent unconformity interpreted as recording initial ice sheet advance across the plateau prior to the early Pliocene. See Main Text Figure 1 for profile location.

Table S5, **next two pages**. Tectonic and stratigraphic events related to the development of the Antarctic Circumpolar Current. References cited are numbers 46 through 75.

Late Jurassic-Early Cretaceous: Earliest age suggested for Central Scotia Sea floor by Eagles (2010).

- **Late Jurassic-Early Cretaceous**: Age of initiation of stretching between Australia and East Antarctica, ~153 Ma (Wilcox and Stagg, 1990) with initiation of oceanic sea floor spreading by ~95 Ma (Tikku and Cande, 2000) although Cande and Stock (2005) now put oldest identified seafloor spreading anomaly as C33y (79 Ma).

- **ca. 58-49 Ma**: extensional opening of Rio Bueno-De Agostini depocenters near Staten Island/Tierra del Fuego believed by Ghiglione et al. (2008) to be indication of initial extension in development of Drake Passage.

- **ca. 56-54 Ma**: Last mammal dispersal from South America to the Antarctic Peninsula (Woodburne and Zinsmeister, 1984; Reguero and Marenssi, 2010), evidence of initiation of shallow seaway in future Drake Passage.

- **prior to Early Eocene, 56 Ma:** South Tasman Saddle, a100+ km wide, 2 km deep seaway between Tasmania and the South Tasman Rise, clears East Antarctica (Lawver et al., in press).

- **ca. 45-35 Ma**: Onset of rapid cooling, ~48 Ma with exhumation of the Fuegian (southernmost) Andes beginning no later than 45 Ma (Gombesi et al., 2009).

- **ca. 41 Ma**: Nd-isotopes of fossil fish teeth indicate evidence of possible penetration of Pacific-derived seawater through Drake Passage into the Atlantic sector of Southern Ocean (Scher and Martin, 2006).

- **ca. 41-34.7 Ma**: age of seafloor-spreading in Dove Basin based on marine magnetic anomaly identifications and depth-to-age models (Eagles et al., 2006)

- **ca. 40-29.7 Ma**: stretching of Powell Basin estimated to have begun by 40 Ma with sea floor spreading magnetic anomalies identified as chrons C11 to C6AA (29.8-21.8 Ma) according to Eagles & Livermore, 2002.

- **ca. 40 Ma**: age of initial deep water passage between South Tasman Rise and East Antarctica (Lawver et al., in press)

- **ca. 39 Ma**: sediment provenance shift in the eastern Magallanes basin indicating rapid exhumation of Cordillera Darwin complex (Barbeau et al., 2009).

- **ca. 36-33.5 Ma**: alternating dominances of cool-water nannofossil taxa at Maude Rise, ODP Site 689 (36.41-33.54 Ma), synchronous with Kerguelen, ODP Site 744 (35.80-33.54 Ma) found by Persico and Villa (2004).

- **ca. 34 Ma**: age of opening between remnant of Ninety East Ridge and Kerguelen Plateau to develop continuous passage directed to the southeast (Lawver et al., in press)

- **ca. 34-30 Ma**: Preferred Protector Basin seafloor spreading model of Eagles et al. (2006), although they offer a second, older model with age of seafloor spreading based on magnetic anomaly identification and depth-to-age of ~48.5-41 Ma. Galindo-Zaldivar et al. (2006) suggest Protector Basin models based on magnetic anomaly identifications of 23.8-20.1 Ma, 22-17.6 Ma, and 17.4-13.8 Ma. Hill and Barker (1980) modeled their marine magnetic anomalies as chrons C5D to C5AA (17.5 Ma to 13.1 Ma).

- **ca. 33-30 Ma**: reduced sedimentation at ODP Site 1090, 33.4-30.2 Ma and a hiatus around 32 Ma attributed to opening of Drake Passage and ending of opal pulse at ~33 Ma (Diekmann et al., 2004).

- **32.8 Ma:** permanent change in Barium concentration record at ODP Site 1090 in the southeastern Atlantic is used as indication of initial deep-water circulation resulting from opening of Drake Passage (Latimer and Filippelli, 2002).

- **ca. 31-30 Ma**: Initiation of ACC based on depositional hiatus at Maud Rise Site, ODP 690C, which is coeval with hiatuses seen on two Kerguelen Plateau sites, 744A and 748B and with time of decrease in sedimentation rate at the shallower ODP Site 689 on Maud Rise (Florindo and Roberts, 2005).

- **29.7-21.8 Ma:** seafloor-spreading (drift phase) of Powell Basin opening (Eagles and Livermore, 2002).

- **ca. 29 Ma**: oldest proposed age for West Scotia Sea oceanic crust Chron C10 (LaBrecque and Rabinowitz, 1977) although Barker and Burrell (1977) and Eagles et al. (2005) only show C8 (~26.5 Ma) as the oldest and Eagles et al. (2005) indicate a possible C9, Lodolo et al. (1997) show a possible C9 and C10 and Lodolo et al. (2006) show definite C10 (28.4 Ma) and C9 in the western sector of the West Scotia Sea.

- **>26 Ma**: age of Central Scotia Sea (Eagles et al., 2005), although Hill and Barker (1980) identified the east-west trending magnetic anomalies as either chrons C12 to C6C (30.9 to 24.6 Ma) or chrons C6C to C4A (24 Ma to 9 Ma).

- **ca. 26 Ma**: oldest consistently identifiable magnetic anomaly (chron C8) in West Scotia Sea (Barker and Burrell, 1977; Eagles et al., 2005).

- **ca. 23.9 Ma**: Grain size change found at ODP Site 1170 (South Tasman Rise) indicates initiation of ACC (Pfuhl and McCave, 2005).

- **ca. 15 Ma**: oldest consistently identifiable magnetic anomaly (Chron C5B) in East Scotia Sea (Larter et al., 2003), although Livermore (2003) speculates that there may be older anomalies, perhaps as old as C6A (~21 Ma).

- **ca. 15 Ma**: time of initial collision of Australia with Southeast Asia (Lee and Lawver, 1995) and reduction of Circum-tropical circulation through the Indonesian Seaway.

References Cited

1. Shipboard Science Party (2006) SHALDRIL II 2006 Cruise Report (NBP06-02A). <http://shaldril.rice.edu/PDFs/NBP0602A.pdf>.

2. Warny S, Askin RA (in press-a) in *Tectonic, Climatic and Cryospheric Evolution of the Antarctic Peninsula*, eds Anderson JB, Wellner JS (AGU Special Paper).

3. Warny S, Askin RA (in press-b) in *Tectonic, Climatic and Cryospheric Evolution of the Antarctic Peninsula*, eds Anderson JB, Wellner JS (AGU Special Paper).

4. Gradstein FM, Ogg JG, Smith AG (2004) *A Geologic Timescale 2004*, Cambridge University Press, Cambridge, UK, 610 pp.

5. Shipboard Science Party (2005) SHALDRIL 2005 Cruise Report (NBP05-02). <http://SHALDRIL.rice.edu/PDFs/total.pdf>.

6. Smith RT, Anderson JB, (in press) in *Tectonic, Climatic and Cryospheric Evolution of the Antarctic Peninsula*, eds Anderson JB, Wellner JS (AGU Special Paper).

7. Baldauf JG, Barron JA (1991) in *Proceedings of the Ocean Drilling Program, Scientific Results* 119: 547-598.

8. Barron JA, Fourtanier E., Bohaty SM (2004) Oligocene and earliest Miocene diatom biostratigraphy of ODP Leg 199 Site 1220, Equatorial Pacific. *Proc. ODP, Sci. Results* 199: 1-25: <http://www-odp.tamu.edu/publications >.

9. Berggren WA, Kent DV, Swisher CC III, Aubry M-P (1995) A revised Cenozoic geochronology and chronostratigraphy. *Special Publication - SEPM (Society for Sedimentary Geology* 54: 129-212.

10. Bohaty SM, Wise, SW Jr., Duncan RA, Moore CL, Wallace PJ (2003) Neogene diatom biostratigraphy, tephra stratigraphy, and chronology of ODP Hole 1138A, Kerguelen Plateau. *Proc. ODP, Sci. Results*, *183*, 1-53, <http://www-odp.tamu.edu/publications/183_SR/VOLUME/CHAPTERS/016.PDF>.

11. Censarek B, Gersonde R (2002) Miocene diatom biostratigraphy at ODP Sites 689, 690, 1088, 1092 (Atlantic sector of the Southern Ocean). *Marine Micropaleontology* 45: 309-356.

12. Cody RD, Levy RH, Harwood DM, and Sadler PM (2008) Thinking outside the zone: High-resolution quantitative diatom biochronology for the Antarctic Neogene. *Palaeogeography Palaeoclimatology Palaeoecology* 260: 92-121, doi:10.1016/j.palaeo.2007.08.020.

13. Gersonde RE, Burckle LH (1990) Neogene diatom biostratigraphy of ODP Leg 113, Weddell Sea (Antarctic Ocean). *Proc. ODP, Sci. Results* 113, 761-789.

14. Gombos AM Jr., Ciesielski PF (1983) Late Eocene to early Miocene diatoms from the Southwest Atlantic. *Init. Reports, DSDP 71*: 583-634.

15. Hajós M (1976) Upper Eocene and lower Oligocene diatomaceae, archaeomonadaceae, and silicoflagellatae in southwestern Pacific sediments, DSDP Leg 29, *Init. Reports, DSDP*, *35*, 817-884.

16. Harwood DM (1989) Siliceous microfossils, in *Antarctic Cenozoic History from the CIROS-1 Drillhole, McMurdo Sound*, edited by P. J. Barrett, DSIR Bulletin 245: pp. 67-97.

17. Harwood DM Maruyama T (1992) Middle Eocene to Pleistocene diatom biostratigraphy of Southern Ocean sediments from the Kerguelen Plateau, Leg 120, *Proc. ODP, Sci. Results*, *120*, 683-733.

18. Harwood DM, Bohaty SM (2001) Early Oligocene siliceous microfossil biostratigraphy of Cape Roberts Project core CRP-3, Victoria Land Basin, Antarctica, *Terra Antartica*, *8*(4): 315-338.

19. Majewski W, Bohaty SM (2010) Surface-water cooling and salinity decrease during the Middle Miocene climate transition at Southern Ocean ODP Site 747 (Kerguelen Plateau), *Marine Micropaleontology*, *74*, 1-14, doi:10.1016/j.marmicro.2009.10.002.

20. Olney MP, Scherer RP, Harwood DM, Bohaty SM (2007) Oligocene–early Miocene Antarctic nearshore diatom biostratigraphy, *Deep-Sea Research II*, *54*: 2325–2349, doi:10.1016/j.dsr2.2007.07.020.

21. Poore RZ, et al. (1983) Late Cretaceous–Cenozoic magnetostratigraphic and biostratigraphic correlations for the South Atlantic Ocean, Deep Sea Drilling Project Leg 73, *Init. Reports, DSDP*, *73*, 645–655.

22. Roberts AP, et al. (2003) Magnetostratigraphic calibration of Southern Ocean diatom datums from the Eocene-Oligocene of Kerguelen Plateau (Ocean Drilling Program sites 744 and 748), *Palaeogeography, Palaeoclimatology, Palaeoecology*, *198*: 145-168.

23. Scherer RP, Bohaty SM, Harwood DM (2000) Oligocene and lower Miocene siliceous microfossil biostratigraphy of Cape Roberts Project Core CRP-2/2A, Victoria Land Basin, Antarctica, *Terra Antartica*, *7*(4-5): 417-442.

24. Whitehead JM, Bohaty SM (2003) Data Report: Quaternary–Pliocene diatom biostratigraphy of ODP Sites 1165 and 1166, Cooperation Sea and Prydz Bay, *Proc.*

ODP, Sci. Results, *188*, 1-25, <http://www-odp.tamu.edu/publications/188_SR/VOLUME/CHAPTERS/008.PDF>.

25. Williams GL, Brinkhuis H, Pearce MA, Fensome RA, Weegink JW (2004) *Proc. ODP, Sci. Results*, *189*, 1-98, <http://www-odp.tamu.edu/publications/189_SR/VOLUME/CHAPTERS/107.PDF>.

26. Wilson GS, et al. (2000) Chronostratigraphy of CRP-2/2A, Victoria Land Basin, Antarctica, *Terra Antarctica 7*(4-5): 647-654.

27. Wilson GS, et al. (2002) Integrated chronostratigraphic calibration of the Oligocene-Miocene boundary at 24.0 ± 0.1 Ma from the CRP-2A drill core, Ross Sea, Antarctica, *Geology 30*(11): 1043-1046.

28. Winter DM, Iwai M (2002) Data report: Neogene diatom biostratigraphy, Antarctic Peninsula Pacific margin, ODP Leg 178 rise sites, *Proc. ODP, Sci. Results*, *178*, 1-24, <http://www-odp.tamu.edu/publications/178_SR/VOLUME/CHAPTERS/SR178_29.PDF>.

29. Wise SW Jr. (1983) Mesozoic and Cenozoic calcareous nannofossils recovered by Deep Sea Drilling Project Leg 71 in the Falkland Plateau region, Southwest Atlantic Ocean, *Init. Reports, DSDP*, *71*(2), 481-550.

30. Zielinski U, Gersonde R (2002), Plio-Pleistocene diatom biostratigraphy from ODP Leg 177, Atlantic sector of the Southern Ocean, *Marine Micropaleontology*,*45*(3-4),:225-268.

31. Ehrmann W, Setti M, Marinoni L (2005) Clay minerals in Cenozoic sediments off Cape Roberts (McMurdo Sound, Antarctica) reveal palaeoclimatic history, *Palaeogeography, Palaeoclimatology, Palaeoecology 229*: 187 ‑ 211.

32. Petschick R (2001) MacDiff 4.2.5. http://servermac.geologie.uni‑frankfurt.de/Rainer.html.

33. Biscaye PE (1964) Distinction between kaolinite and chlorite in recent sediments by X‑ray diffraction, *American Mineralogist 49*: 1281 ‑ 1289.

34. Biscaye PE (1965) Mineralogy and sedimentation of recent deep‑sea clay in the Atlantic Ocean and adjacent seas and oceans, *Geological Society of America Bulletin 76*: 803 ‑ 832.

35. Brindley GW, Brown G, eds. (1980), Crystal Structures of Clay Minerals and their X‑Ray Identification, *Mineralogical Society Monograph, 5*, 495 pp

36. Esquevin J (1969) Influence de la composition chimique des illites sur le cristallinité, *Bull. Cent. Rech. Pau S.N.P.A. 3*: 147 - 154.

37. Ehrlich R, Weinberg B (1970) Exact method for the characterization of grain shape, *Jour Sed Pet* 40: 205 - 212.

38. Kennedy S K, Ehrlich R (1985). Origin of shape changes of sand and silt in a high - gradient stream system, *Jour Sed Research* 55: 57 - 64

39. Mazzullo J, Ehrlich R, Pilke OH (1982) Local and distal origin of sands in the Hatteras Abyssal Plain, *Marine Geology* 48: 75 - 88, ISSN 0025 - 3227, DOI: 10.1016/0025 - 3227(82)90130 - X.

40. Dowdeswell J A. (1982) Scanning electron micrographs of quartz sand grains from cold environments examined using Fourier shape analysis, *Jour Sed Research* 52: 1315 - 1323.

41. Ehrlich R, Brown TJ, Yarus JM, Przygocki RS (1980) The origin of shape frequency distributions and the relationship between size and shape, *Jour Sed Pet* 50: 475 - 484.

42. Dowdswell JA, Ozterman LE, Andrews JT (1985) Quartz sand grain shape and other criteria used to distinguish glacial and non - glacial events in a marine core from Frobisher Bay, Baffin Island, N.W.T., Canada. *Sedimentology* 32: 119–132. doi: 10.1111/j.1365 - 3091.1985.tb00496.x

43. Mahaney WC, Vortisch W, Julig P (1988) Relative Differences between Glacially Crushed Quartz Transported by Mountain and Continental Ice - Some Examples from North-America and East-Africa. *Am Jour Sci* 288(8): 810-826 .

44. Mahaney WC (2002) *Atlas of sand grain surface textures and applications* (Oxford University Press, Oxford [England], 237 pp.

45. Sweet DE, Soreghan GS (2010) Application of Quartz Sand Microtextural Analysis to Infer Cold-Climate Weathering for the Equatorial Fountain Formation (Pennsylvanian-Permian, Colorado, USA). *Journal of Sedimentary Research* 80(7-8): 666-677.

46. Barbeau DL, et al. (2009) Detrital-zircon geochronology of the eastern Magallanes foreland basin: Implications for Eocene kinematics of the northern Scotia Arc and Drake Passage, *Earth Planet Sci Lett 20:* 23-45.

47. Barker PF, Burrell J (1977) The opening of the Drake Passage, *Marine Geology* 25: 15-34.

48. Cande SC, Stock J M (2005) Cenozoic reconstructions of the Australia –New Zealand – South Pacific sector of Antarctica; The Cenozoic Southern Ocean: Tectonics, Sedimentation and Climate Change between Australia and Antarctica, eds. Exon N., Kennett J. and Malone M., (American Geophysical Union Geophysical Monograph 151): 5-18.

49. Diekmann B, Kuhn G, Gersonde R, Mackensen A (2004) Middle Eocene to early Miocene environmental changes in the sub-Antarctic Southern Ocean: evidence from biogenic and terrigenous depositional patterns at ODP Site 1090, *Global and Planetary Change* 40: 295–313.

50. Eagles G (2010) The age and origin of the central Scotia Sea: *Geophys J Internat* 183: 587-600.

51. Eagles G, Livermore RA (2002) Opening history of Powell Basin, Antarctic Peninsula, *Marine Geol*ogy 185: 197–207.

52. Eagles GRA, Livermore RA, JD, Fairhead JD, Morris P (2005) Tectonic evolution of the west Scotia Sea: *J. Geophys. Res. 1*10 B02401, doi:10.1029/ JB2004003154.

53. Eagles G, Livermore RA, Morris P (2006) Small basins in the Scotia Sea: The Eocene Drake Passage gateway, *Earth Planet Sci Lett* 242: 343-353.

54. Florindo F, Roberts AP (2005) Eocene-Oligocene magnetobiochronology of ODP Sites 689 and 690, Maud Rise, Weddell Sea, Antarctica, *Geol Soc Amer Bull* 117: 46-66.

55. Galindo-Zaldıvar J, Bohoyo F, Maldonado A, Schreider AA, Surinach E, Vazquez JT (2006) Propagating rift during the opening of a small oceanic basin: the Protector Basin (Scotia Arc, Antarctica), *Earth Planet Sci Lett* 241**:** 398-412.

56. Ghiglione MC, Yagupsky D, Ghidella M, Ramos VA (2008) Continental stretching preceding the opening of the Drake Passage: evidence from Tierra del Fuego, *Geology* 36**:** 643-646.

57. Gombosi DG, Barbeau DL, Garver JI (2009) New thermochronometric constraints on the rapid Paleogene uplift of the Cordillera Darwin complex and related thrust sheets in the Fuegian Andes, *Ter Nova* 21: 507-515.

58. Hill IA, Barker PF (1980) Evidence for Miocene back-arc spreading in the central Scotia Sea, *Geophys J R Astr Soc*, 63: 427-440.

59. LaBrecque JL, Rabinowitz PD (1977) Magnetic anomalies bordering the continental margin of Argentina, American Association Petroleum Geologists Map 826.

60. Larter RD, Vanneste LE, Morris P, Smythe DK (2003) Structure and tectonic evolution of the South Sandwich arc. Larter RD and Leat PT eds, Intra-Oceanic Subduction Systems: Tectonic and Magmatic Processes, *Geol Soc London Spec Pub* 219: 255-284.

61. Latimer JC, Filippelli GM (2002) Eocene to Miocene terrigenous imports and export production: geochemical evidence from ODP Leg 177, Site 1090, *Palaeogeography, Palaeoclimatology, Palaeoecology* 182: 151-164.

62. Lawver LA, Gahagan LM, Dalziel IWD (in press) A Different Look at Gateways – Drake Passage and Australia/Antarctica, in Tectonic, climatic and cryospheric evolution of the Antarctic Peninsula, eds. Anderson JB and Wellner JS (American Geophysical Union Special Paper).

63. Lee TY, Lawver LA (1995) Cenozoic plate reconstruction of the Southeast Asia region, *Tectonophysics* 251: 85-138.

64. Livermore R (2003) in Intra-Oceanic Subduction Systems: Tectonic and Magmatic Processes, *eds* Larter, R.D. ,Leat, P.T., (Geol Soc London Spec Pub 219) 315- 331.

65. Livermore RA, Nankivell AP, Eagles G, Morris P (2005) Paleogene opening of Drake Passage. *Earth Planet. Sci. Lett* 236: 459-470.

66. Livermore R, Hillenbrand CD, Meredith M, Eagles G (2007) Drake Passage and Cenozoic climate: An open and shut case?. *Geochem Geophys Geosyst 8*: Q01005.

67. Lodolo E, Coren F, Schreider AA, Ceccone G (1997) Geophysical evidence of a relict oceanic crust in the southwestern Scotia Sea, *Mar Geophys Res* 19: 439-450.

68. Lodolo E, Donda F, Tassone F (2006) Western Scotia Sea margins: Improved constraints on the opening of the Drake Passage, *Jour Geophys Res* 111: B06101, doi:10.1029/2006JB004361, 14 p.

69. Persico D, Villa G (2004) Eocene-Oligocene calcareous nannofossils from Maud Rise and Kerguelen Plateau (Antarctica): paleoecological and paleoceanographic implications, *Marine Micropaleontology*, 52: 153-179.

70. Pfuhl HA, McCave IN (2005) Evidence for late Oligocene establishment of the Antarctic Circumpolar Current, *Earth Planet Sci Lett* 235: 715-728.

71. Reguero, MA, Marenssi SA (2010) in The Paleontology of Gran Barranca - Evolution and Environmental Change through the Middle Cenozoic of Patagonia, eds Madden R., Carlini A, Vucetich MG, Kay RF (Cambridge University Press, Cambridge, U.K.), pp 383-397.

72. Scher HD, Martin EE (2006) Timing and climatic consequences of the opening of Drake Passage, *Science 312*: 428–430.

73. Tikku AA, Cande SC, (2000) On the fit of Broken Ridge and Kerguelen plateau, *Earth Planet Sci Lett* 180: 117-132.

74. Wilcox JB, Stagg HMJ (1990) Australia's southern margin: a product of oblique extension, *Tectonophysics* 173: 269-281.

75. Woodburne MO, Zinsmeister WJ (1984) The first land mammal from Antarctica and its biogeographic implications, *Jour. Paleontology* 58: 913-948.